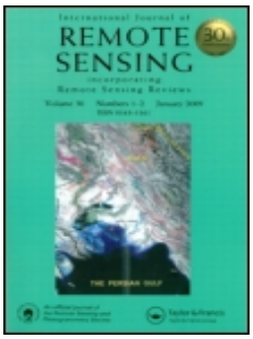

International Journal of Remote Sensing

ISSN: 0143-1161 (Print) 1366-5901 (Online) Journal homepage: www.tandfonline.com/journals/tres20

Using NOAA AVHRR and SPOT VGT data to estimate surface parameters: application to a mesoscale meteorological model

N. Pineda Corresponding author, O. Jorba, J. Jorge & J. M. Baldasano

To cite this article: N. Pineda Corresponding author, O. Jorba, J. Jorge & J. M. Baldasano (2004) Using NOAA AVHRR and SPOT VGT data to estimate surface parameters: application to a mesoscale meteorological model , International Journal of Remote Sensing, 25:1, 129-143, DOI: 10.1080/0143116031000115201

To link to this article: https://doi.org/10.1080/0143116031000115201

INT. J. REMOTE SENSING, 10 JANUARY, 2004,
VOL. 25, NO. 1, 129–143

Taylor & Francis
Taylor & Francis Group

Using NOAA AVHRR and SPOT VGT data to estimate surface parameters: application to a mesoscale meteorological model

N. PINEDA*†, O. JORBA‡, J. JORGE† and J. M. BALDASANO‡

†Department of Applied Physics, Escola Universitària Politècnica de Manresa (EUPM), Universitat Politècnica de Catalunya (UPC), Av. Bases Manresa 61-73, 08240 Manresa, Spain
‡Laboratory of Environmental Modeling, Escola Tècnica Superior d'Enginyeria Industrial de Barcelona (ETSEIB), Universitat Politècnica de Catalunya (UPC), Av. Diagonal 647, 08028 Barcelona, Spain

Abstract. The mesoscale numerical weather prediction model MM5, the 5th generation Pennsylvania State University/NCAR Mesoscale Model, uses a global land-use map to set the physical parameters on the surface characteristics to model the soil-atmosphere processes. These parameters are albedo, emissivity, thermal inertia, roughness length and soil moisture. A new estimation of soil parameters is done for the north-east of the Iberian Peninsula from an AVHRR data set of year 2000. The new values are introduced into MM5 via a new land-use map, the recent NATLAN 2000-CORINE land-use map, in order to incorporate the last decade land-cover changes. The model is tested with the original and the CORINE land-use map to evaluate the sensitivity to land-use changes and new physical soil parameters definition. Results show clear local differences in some meteorological variables as wind fields or updraft movements, but comparisons with ground measurements do not lead to a clear improvement in the model general performance.

1. Introduction

Correctly treating the land surface properties is becoming increasingly important for meteorological models to be able to capture local mesoscale circulation induced by land surface forcing (Chen and Dudhia 2001). Several mesoscale models, like the fifth-generation Pennsylvania State University/NCAR Mesoscale Model (MM5) used in this study, rely on albedo, emissivity, thermal inertia, roughness length and soil moisture data sets derived from land-use maps. The simple surface parameters scheme of the model specifies them according to land use category and season. The accuracy of land-use information is important to obtain accurate simulations.

MM5 (Dudhia 1993) uses the USGS global land-use map (Anderson *et al.* 1976) to set the physical parameters on the surface characteristics, a 10-year old land-use map that was created with multitemporal 1-km AVHRR NDVI data (1992–1993). To incorporate the last decade land-cover changes, the recent CORINE land-use

*Corresponding author; e-mail: npineda@fa.upc.es

International Journal of Remote Sensing
ISSN 0143-1161 print/ISSN 1366-5901 online
http://www.tandf.co.uk/journals

map of the European Environment Agency NATLAN information package (EEA 2000) was used in the simulations instead of the original map.

Surface parameters (albedo, emissivity and thermal inertia) were estimated for the working region from an AVHRR data set of year 2000, and mean values for the CORINE land-use classes were calculated for the four seasons. As soil moisture and roughness can not be estimated with optical remote sensing sensors, a category equivalence between land-use maps was established, in order to use the original MM5 tabulated roughness and moisture values with the new land-use map.

2. Study location

The location of the present study is situated in the north-east of the Iberian Peninsula (figure 1). This region is characterized with very complex topography, a high mountain range to the north of the area, with extended mountains to the south-west and an important river-valley canalisation going from the north-west to the east flowing into the Mediterranean sea. The sea is another particularity of the region, with a large coastline.

3. Surface parameter estimation

3.1. *AVHRR processing*

A selection of 70 afternoon pass and 55 morning pass NOAA-14 AVHRR L1B images were used in this study. Such images were provided by the *Centro de Recepción, Proceso, Archivo y Distribución de Imágenes de Observación de la Tierra* (CREPAD). Before surface parameter estimation some corrections were applied:

Step 1. Calibration. Because of sensor degradation after launch, it was necessary to apply time-dependent calibration gains and offsets, obtained from NOAA (1998), to derive the top of atmosphere (TOA) radiance for AVHRR 1 and 2 channels.

Step 2. TOA reflectance for AVHRR channels 1 and 2. A lambertian correction (Teillet 1992) was used to transform radiance to reflectance.

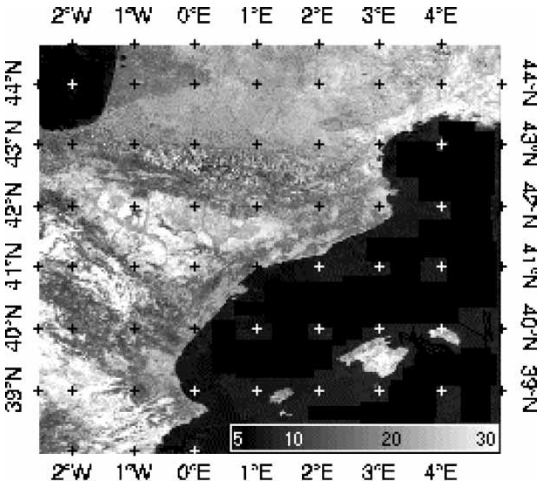

Figure 1. Estimated albedo (%) for August 2000 in the D3 domain of MM5 over NE Spain.

Step 3. Atmospheric correction. The SMAC algorithm (Rahman and Dedieu 1994) was employed to convert TOA reflectance to surface reflectance of each image. SMAC input data, like water vapour content and columnar ozone content was derived from the NOAA-14 TOVS sensor, data provided by the ATMOS User Center of the German Remote Sensing Data Center (DFD). Aerosol optical depth (at 550 nm) was obtained from the Aerosol Robotic Network (AERONET) (Holben *et al*. 1998). For the thermal channels, a split-window technique was used. Day and night land surface temperature were calculated with the Sobrino and Raussoni (2000) algorithm. Input data are channels 4 and 5 brightness temperature, surface emissivity and water vapour, obtained from the morning and afternoon passes of the NOAA TOVS.

Step 4. Identification of cloud contaminated pixels and image compositing. In order to create cloud-free monthly mean images, clouds were filtered using a regional adaptation of the threshold procedure proposed by Derrien *et al*. (1993). Once the clouds were masked, monthly composites were calculated, applying the mean for the non-contaminated pixels, channel-by-channel. Surface parameters were estimated from these monthly composites.

3.2. *Geophysical surface parameter estimation*

Albedo was estimated assuming lambertian reflection. To derive broad-band albedo from AVHRR, a narrow-band to broad-band conversion method (Saunders 1990) that combines weighted AVHRR channels 1 and 2 was used. From the channel weights proposed by different authors, the ones estimated for the Iberian Peninsula by Valiente *et al*. (1995) were used.

Emissivity at 9 nm was calculated using the Valor and Caselles (1996) method, which estimate emissivity from AVHRR NDVI images.

Thermal Inertia (TI) was estimated according to the simple formulation for calculating TI from remote sensing data, given by Price (1977). The Sobrino and El Kharraz (1999) Price's model adaptation was used. Calculated TI values with AVHRR were higher than USGS ones for all the land-use categories, especially in coastal and high altitude regions as shown in figure 2. Low altitude flat and continental regions are the most similar to MM5 global TI values. It seems that sea and mountain effects in TI are not contemplated in the MM5 tabulated TI values.

4. Land-use category equivalence

Albedo, emissivity and TI were derived from the AVHRR data set, but roughness and soil moisture can not be estimated with optical sensors. To run the simulation in MM5 with the CORINE land-use map, it was necessary to obtain an estimation of these surface parameters for the CORINE categories. In order to relate current tabulated MM5 USGS roughness and moisture values to the new land-use categories, equivalence between the land-use maps was carried out. The NDVI vegetation index was used to establish category equivalencies, making the assumption that surface roughness is mainly due to vegetation cover and that there is a good relation between soil moisture and vegetation presence.

For the land-use category equivalence study, a set of 36 SPOT VGT S_{10} (10-day synthesis) NDVI images of the year 2000 was used. Although NDVI vegetation index can be calculated with AVHRR images, the SPOT VGT S_{10} data set has more images (one every 10 days), better calibration and geographical quality than

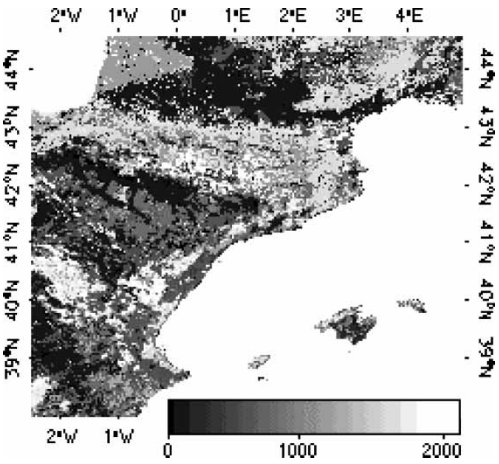

Figure 2. Differences (CORINE – USGS) in thermal inertia $\left(\mathrm{W\,m^{-2}\,k^{-1}\,s^{1/2}}\right)$ over land for August 2000.

AVHRR data, thus it is more suitable for annual vegetation cycle variation analysis.

Calculated parameters for the CORINE categories are shown in table 1. Winter and summer periods correspond to three-month means. The equivalence between land-use categories is shown on the right part of table 1. The final column corresponds to Gower metric statistics (Gower 1971), used to compare annual NDVI cycle similarities and to establish category equivalencies. As Gower statistics value gets lower, annual NDVI patterns between categories are more similar.

In figure 3 annual NDVI cycles of some CORINE and USGS land-use categories are represented. Cropland categories are represented in figure 3(*a*). CORINE 'Non-Irrigated Arable Land' (cat.12) has a similar NDVI annual pattern with its comparable class in USGS, dry crops (cat.102), but with higher NDVI values. The same occurs for the irrigated crops (CORINE cat.13 and USGS cat.103), but rice fields (CORINE cat.14) have a completely different NDVI annual pattern. According to Gower statistics roughness and moisture values for rice fields were taken from USGS cat.103 (Gower: 21.7). Figure 3(*b*) shows a good equivalence between USGS cat.111 'Deciduous Broadleaf Forest' and CORINE cat.23 'Broad-Leaved Forest' (Gower: 5.7) and a less good equivalence between USGS cat.114 'Evergreen Needleleaf Forest' and CORINE-24 'Coniferous Forest' (Gower: 20,4). Shrubland categories are represented in figure 3(*c*). CORINE 'Sclerophyllous Vegetation' (cat.28) should theoretically correspond to USGS 'Shrubland' (cat.108), but according to the NDVI pattern and Gower metrics (21.3 for cat.109 and 45.3 for cat 108), it seems more appropriate to take values of roughness and moisture from class 'Mix Shrubland/Grassland' (cat.109) for the 'Sclerophyllous Vegetation' category. Finally, besides Shrubland categories, grassland (USGS cat.107) is represented in figure 3(*c*). The NDVI is quite different between summer and winter periods in this category, due to the snow presence between November and April.

Table 1. Surface parameters for CORINE land-use categories for winter (W) and summer (S) and equivalencies with USGS land-use map. The third column is percent of category presence in the land surface of D3 domain.

CORINE	Category description	%	Albedo (%)		Moisture avail. (%)		Emissiv. (% at 9 μm)		Roughness length (cm)		Thermal Inertia ($W m^{-2} k^{-1} s^{1/2}$)		Equivalencies			
			W	S	W	S	W	S	W	S	W	S	CORINE	USGS	USGS category description	GOWER
1–11	Urban	0.43	16.8	17.8	10	10	93.5	93.7	50	50	2283	2895	1–11	101	Urban and Built-Up Land	6.2
12	Non-Irrigated Arable Land	21.77	18.4	20.7	60	30	96.0	95.8	5	15	2064	2332	12	102	Dryland Cropland and Pasture	15.2
13	Permanently Irrigated Land	3.23	19.7	20.5	50	50	95.4	96.5	5	15	1582	2322	13	103	Irrigated Cropland and Pasture	11.2
14	Rice Fields	0.18	15.7	17.0	50	50	92.8	97.5	5	15	2618	3977	14	103		21.7
15	Vineyards	3.91	18.5	19.9	60	35	95.2	95.6	20	20	1906	2321	15	106		23.5
16	Fruit Trees & Berry Plantations	1.97	16.5	17.1	60	35	96.4	95.9	20	20	2097	2831	16	106	Crops/Wood mosaic	27
17	Olive Groves	0.51	15.8	17.1	60	35	96.4	95.3	20	20	2010	2537	17	106		15
18	Pastures	2.32	16.0	17.1	60	30	97.6	98.9	5	15	2636	3348	18	102	Dryland Cropland and Pasture	36.1
19	Annual Crops & Permanent Crops	0.50	18.5	20.4	60	35	97.1	93.7	20	20	2093	2410	19	106		22.6
20	Complex Cultivation Patterns	9.21	17.4	18.8	60	35	96.5	96.7	20	20	2219	2619	20	106	Crops/Wood mosaic	33.9
21	Mixed Agriculture & Natural Vegetation	5.94	17.8	19.4	60	35	95.7	95.0	20	20	1655	2211	21	106		24.5
22	Agro-Forestry Areas	0.08	17.8	19.4	60	35	95.7	95.0	20	20	1655	2211	22	106		19
23	Broad-Leaved Forest	10.03	14.4	16.1	60	30	97.1	98.5	50	50	2771	3269	23	111	Deciduous Broadleaf Forest	5.7
24	Coniferous Forest	12.56	14.1	14.3	60	30	97.3	97.4	50	50	2394	2983	24	114	Evergreen Needleleaf Forest	20.4
25	Mixed Forest	3.15	14.1	14.8	60	30	97.4	98.4	50	50	2659	3283	25	115	Mixed Forest	4.8

Table 1. *(Continued)*

CORINE	Category description	%	Albedo (%) W	Albedo (%) S	Moisture avail. (%) W	Moisture avail. (%) S	Emissiv. (% at 9 μm) W	Emissiv. (% at 9 μm) S	Roughness length (cm) W	Roughness length (cm) S	Thermal Inertia ($W m^{-2} k^{-1} s^{1/2}$) W	Thermal Inertia ($W m^{-2} k^{-1} s^{1/2}$) S	Equivalencies CORINE	Equivalencies USGS	Equivalencies USGS category description	Equivalencies GOWER
26	Natural Grassland	4.30	17.7	17.2	30	15	96.1	98.0	0.10	0.12	2505	2889	26	107	Grassland	42
27	Moors & Heathland	1.19	16.0	16.4	25	15	97.4	98.4	10	11	2500	3216	27	109		28.4
28	Sclerophyllous Vegetation	6.41	15.6	15.8	25	15	96.4	96.0	10	11	2135	2575	28	109	Mix Shrubland/ Grassland	21.3
29	Transitional Woodland-Shrub	6.06	15.4	15.6	25	15	96.7	96.5	10	11	2112	2657	29	109		11.5
30	Beaches, Dunes & Sand Plains	0.06	16.8	17.1	5	2	94.5	96.9	10	10	2752	2778	30	119		66.4
31	Bare Rock	0.62	17.3	16.9	5	2	96.2	96.5	10	10	2619	2948	31	119	Barren or Sparsely Vegetated	55.8
32	Sparsely Vegetated Areas	0.98	19.6	21.1	5	2	95.1	94.3	10	10	1631	2023	32	119		72
33	Burnt Areas	0.19	13.3	13.8	5	2	97.0	96.4	10	10	1966	2600	33	119		113.2
34	Glaciers & Perpetual Snow	0.00	51.3	41.5	95	95	99.7	96.1	5	5	359	418	34	124	Snow or Ice	–
35–38	Inland Marshes Peatbogs, Salines	0.06	14.7	15.5	75	60	94.6	95.8	20	20	2611	3329	35–38	117	Herbaceous Wetlands	–
39	Intertidal Flats	0.01	15.1	15.8	75	80	93.7	95.6	20	20	2802	3901	39	117		–
40–43	Inland Water	0.16	7.8	7.7	100	100	97.8	97.8	0.01	0.01	5916	7116	40–43	116	Water Bodies	–
44	Sea & Ocean	–	7.8	7.7	100	100	97.8	97.8	0.01	0.01	7055	7829	44	116		–

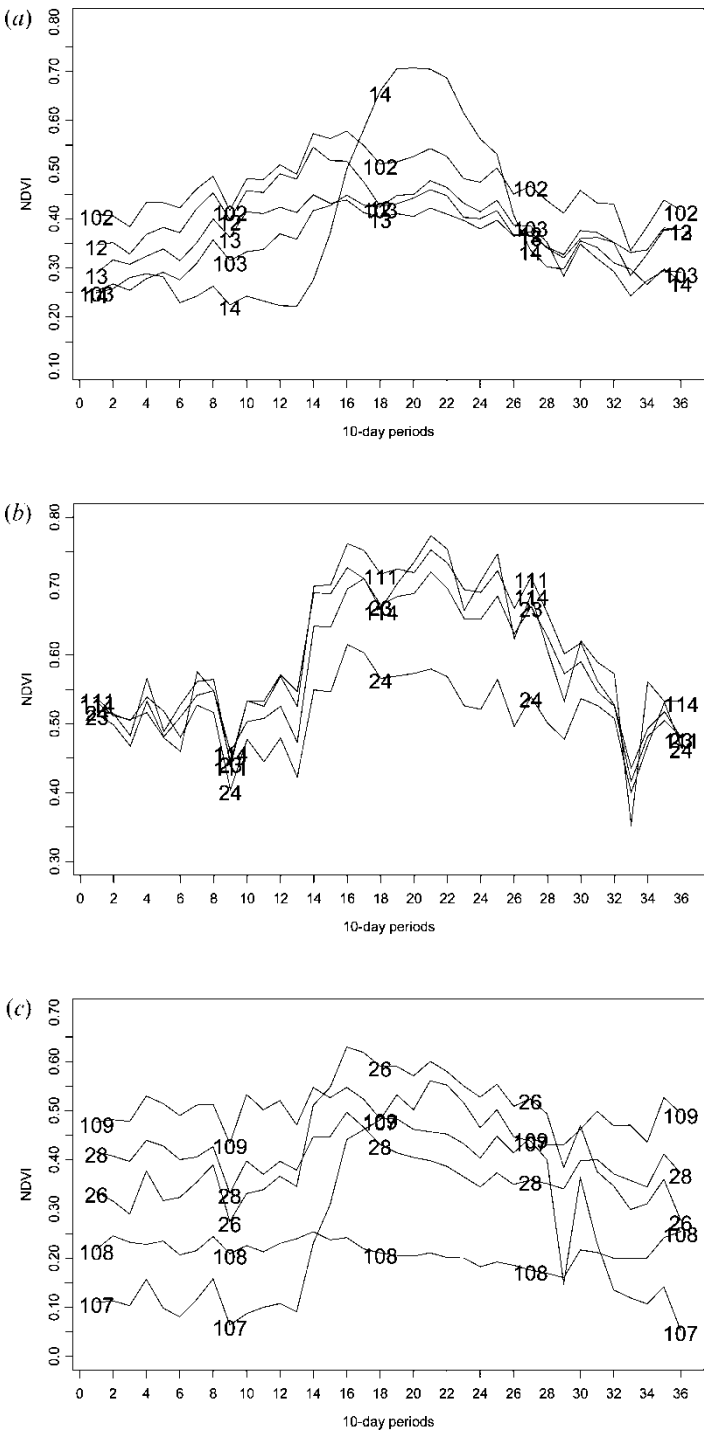

Figure 3. Annual SPOT VGT S_{10} NDVI cycles for year 2000 of some CORINE and USGS land-use categories: (*a*) Cropland categories, (*b*) Forest categories and (*c*) Shrubland categories.

5. Meteorological model

The mesoscale meteorological model used in this study is MM5. It is a community mesoscale model widely used for numerical weather prediction, air quality studies, and hydrological studies. On the smaller meso-beta and meso-gamma scales (2–200 km), MM5 can be applied to studies involving mesoscale convective systems, fronts, land-sea breeze, mountain-valley circulations, and urban heat islands (MMD/NCAR 2001).

Two major changes were introduced into the model in order to evaluate some improvements in its performance. A new set of physical soil properties was introduced to MM5 via a more accurate land-use map. Some modifications were carried out to adapt the new information to the model. These new parameters are tabulated in table 1 for winter and summer cases.

To evaluate the behaviour of MM5 with these modifications, two simulations were performed. A basic case with the default values of physical soil properties and the land-use map of the USGS, and a simulation with the new parameters and the CORINE land-use map. Hereinafter the simulation with the CORINE land-use map and the new physical soil properties will be named CORINE simulation, and the simulation with the default values of MM5, USGS simulation.

5.1. *Model configuration*

Four nested domains were selected (figure 4), which essentially covered Europe (Domain 1, D1), the Iberian Peninsula (Domain 2, D2), NE of the Iberian Peninsula (Domain 3, D3) and Catalonia (Domain 4, D4). D1 has 50×35 grid points in the horizontal with 72 km grid-point spacing. D2 has 61×49 24 km cells. D3 has 93×93 6 km cells. D4 has 151×151 2 km cells. The vertical resolution consisted for all domains of 23 σ-layers, with the lowest one situated approximately at 36 m AGL.

The model uses the Mellor-Yamada scheme as used in the ETA model (Janjic 1994) for the boundary layer parameterization, the Anthens-Kuo and Kain-Fritsch (Kain and Fritsch 1993) cumulus scheme for domains 1 and 2, and no cumulus parameterization for domains 3 and 4. A simple ice explicit moisture scheme, a cloud-radiation scheme, and the five-layer soil model are the other physical parameterizations used in these simulations.

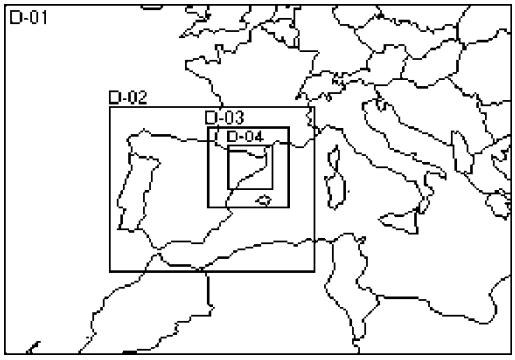

Figure 4. MM5 domain definition over Southern Europe.

Initialization and boundary conditions for the mesoscale model were introduced with analysis data of the European Center for Medium-Range Weather Forecasts (ECMWF) global model. Data were available at a 1° resolution (100 km approx. at the working latitude) at the standard pressure levels every 6 hours.

5.2. *Meteorological situation*

A synoptic situation was studied in order to evaluate the performance of the model working with a new land use map and physical parameters obtained with the methodology explained before. The meteorological case was 14 August 2000. A situation with weak synoptic forcing was chosen, so that mesoscale phenomena induced by the particular topography of the region, and the physical properties of the soil would be dominant.

Synoptic situation of 14 August corresponds to a typical summertime barometric swamp over the Iberian Peninsula. At surface, the high pressure area is centred over the south Atlantic ocean, with the anticyclonic wedge affecting most parts of the Iberian Peninsula, producing a typical barometric swamp along the easterly part of the Peninsula. Surface winds are low. This fact, and the strong daily solar heating, produced the development of mesoscale phenomena. These phenomena in the region are mainly sea breezes, up-slope and down-slope winds and valley channelled winds. The heating during 14 August was so intense that a thermal low started to develop in the south-east of the Iberian Peninsula. In height, a zonal flow blows aloft the Peninsula veering to the south-east having north-westerly winds affecting the north-east of the Iberian Peninsula. The winds aloft exhibit the maximum velocities north-west of the Peninsula.

6. Model results

The new land-use map and the physical soil parameters were introduced to MM5. Three regions of domain 4 are described in order to illustrate the differences produced by those changes. The differences in moisture availability between the two model simulations are displayed in figure 5, with the location of three test regions

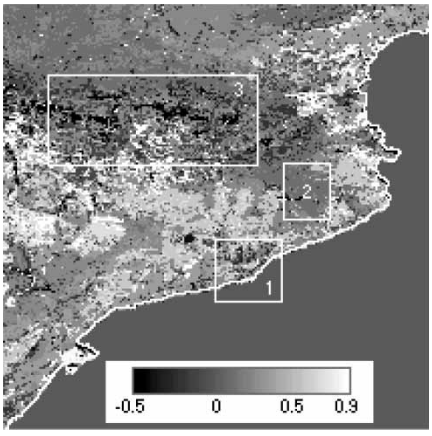

Figure 5. Differences in Moisture Availability (%) between the two MM5 simulations (CORINE-USGS). Test regions: (1) Barcelona Region, (2) Garrotxa Region and (3) Pyrenees.

(1. Barcelona, 2. Garrotxa, 3. Pyrenees). A first area with an introduction of several urban zones around Barcelona city, a second one with a large extension of a land-use homogeneous change, and a third one comprising a mountain chain ranging from 1000 to 3000 m.

6.1. *Barcelona region*

In figure 6(*a*) differences in ground temperature (CORINE-USGS) are displayed. The values are percentages relative to USGS ground temperature. The regions with a new reclassification of the land-use to urban soil appear to be warmer in CORINE simulation. The difference range varies from 25% to −25%. These differences in ground temperature affect air temperature at the first layer of the model in a lower way, with variations at 14 UTC ranging from 2.5% to −1.5% (figure 6(*b*)). Such variations are due to the change of soil physical parameters, changes that are sufficiently important to produce variations in cloud developments, and as a result, precipitation patterns are slightly different.

The variation of surface budgets between the two simulations is able to change the surface and aloft wind fields in several regions of domain 4. Figure 7(*a*) shows the surface wind field of the geographical area of Barcelona obtained with the USGS land-use map at 14 UTC. A sea breeze is well established, blowing inland over the entire domain, with southerly winds veering south-easterly leeward the coast mountain range. Figure 7(*b*) shows the differences between the two surface wind fields simulated by CORINE and USGS land-use map. The arrows are the wind field difference between CORINE and USGS, and the coloured areas represent the differences in wind velocity. With the modifications introduced to MM5, the sea breeze is weaker inland, and over the sea has a more south-westerly component. The differences in the velocity magnitude are lower in comparison to the direction differences. It is important to note that in other regions where convective flows are simulated, surface winds can vary in 5 ms^{-1}. Such differences are due to the modifications of the soil physical parameters, which in turn modify the placement of the vertical thermals that produce the cumulus clouds.

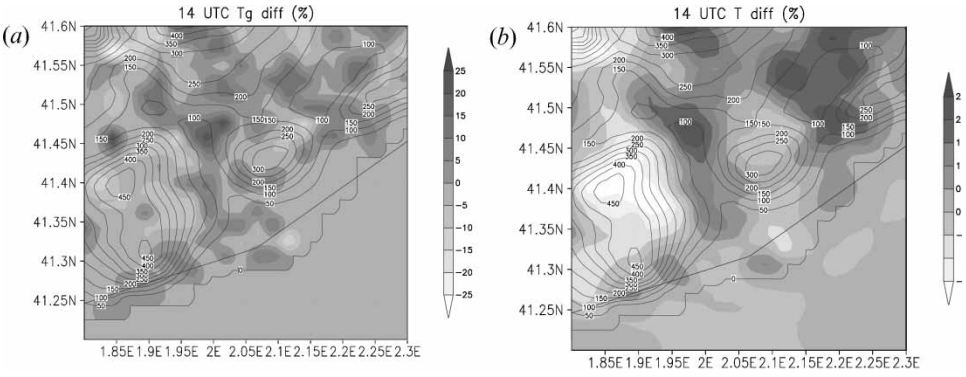

Figure 6. Barcelona Region temperature (°C) differences (CORINE-USGS): (*a*) ground temperature and (*b*) first level temperature.

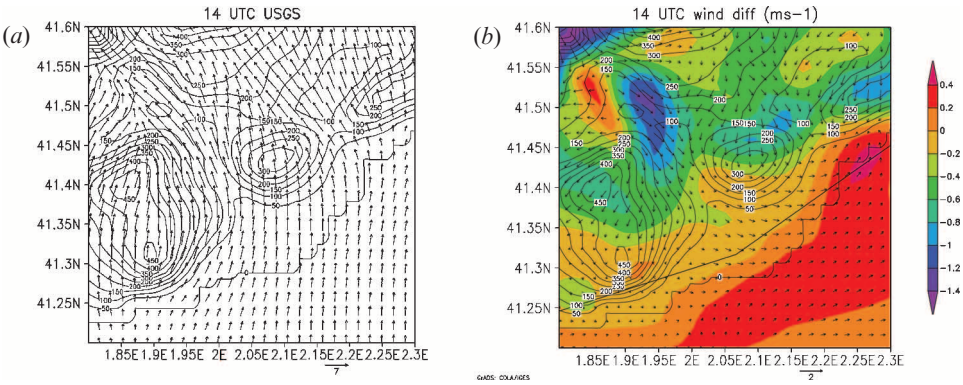

Figure 7. Barcelona region differences (CORINE-USGS) in (*a*) surface wind field of the basic case and (*b*) surface wind field.

6.2. *Garrotxa region*

The change of the land-use map produces a general increase of thermal inertia, roughness length, emissivity and albedo, and a decrease of moisture availability in the Garrotxa Region. In the USGS map, the land-use is cropland-woodland mosaic, and with the implementation of the CORINE land-use map, that region is considered basically as broad-leaved forest. The values of the physical soil parameters with the two maps are tabulated in table 2.

The more important differences in physical parameters reside on thermal inertia and roughness length. With these values, a warmer layer near the ground should be simulated during night with CORINE map, and colder during daytime. However, the model seems to be more sensitive to moisture availability than to the rest of the other parameters.

In figure 8, the evolution of temperature at a location within the region is shown. At night, the ground temperature (*a*) is higher with the CORINE simulation due to the high values of thermal inertia associated to the land-use class of that point, nevertheless, during daytime the temperature with CORINE continues over the USGS one. This performance can be explained due to the lower values of moisture availability, producing a decrease of the latent heat flux. In the evolution of the first layer temperature (*b*) the two simulations have a similar behaviour, with a faster response to a decrease of the incident short wave downward radiation by USGS case, because of the lower value of TI. The decrease of incident radiation is caused by clouds, with slight variations in extension dimension between simulations.

Table 2. Physical parameters for the dominant category in the Garrotxa Region (2) for the two land-use maps.

Land-use category	Albedo (%)	Moisture avail. (%)	Emissivity (% at 9 μm)	Roughness length (cm)	Thermal inertia ($\mathrm{W\,m^{-2}\,k^{-1}\,s^{1/2}}$)
USGS Crop./Woodland mosaic (cat.106)	16	35	93	20	1672
CORINE Broad-leaved forest (cat.23)	16.1	30	98.5	50	3269

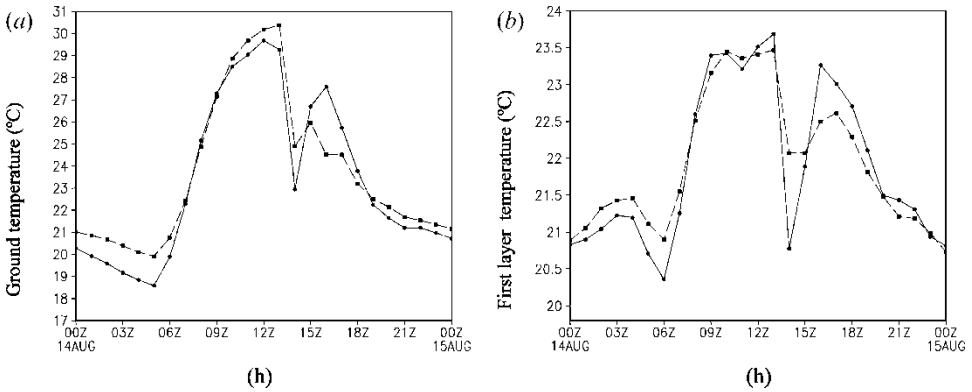

Figure 8. Daily evolution of (*a*) ground temperature (°C) and (*b*) first layer temperature (°C) at 42°8′24″ N 2°30′ E in Garrotxa Region (2) (dashed line CORINE, solid line USGS).

6.3. *Pyrenees*

With the CORINE land-use map and the new values of the physical soil parameters the model simulates higher ground temperatures in the Pyrenees mountain range during all the simulated period. These differences can reach values up to 90% of the value simulated with USGS. That behaviour can be explained due to the low values of moisture availability associated to the high peaks of the Pyrenees with the new reclassification. Complex variations in the wind fields are produced within this region due to the high complexity of the topography and the variations introduced with the new parameters. Note that depending on the location of cumulus development, the aloft winds can vary in an important way. A cross section of the wind field and the mixing ratio is displayed in figure 9, the top panel shows the cross section for the results of the CORINE simulation, and the bottom panel the cross section for the USGS simulation.

The differences are clearly evident, with an important updraft over the middle of

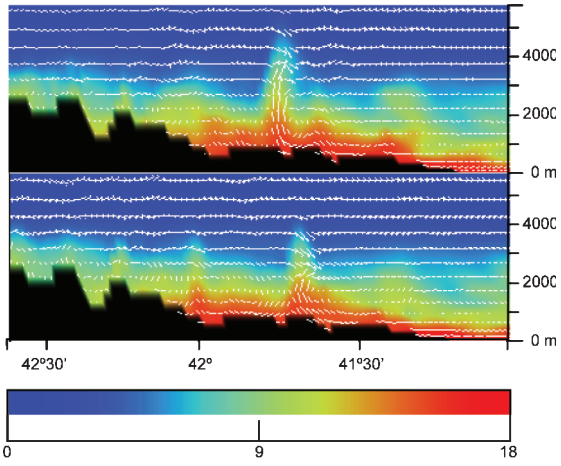

Figure 9. Cross section from north (left) to south (right) of the wind field (white arrows) and the mixing ratio (kg/kg) (coloured scale with topography in black) along 1.55° E at 15 UTC (CORINE upper, USGS bottom panel).

the region injecting moist air aloft in the CORINE simulation. This updraft is less important in the USGS case, with a boundary layer warmer and dryer in comparison with the CORINE one.

6.4. *Measurement comparison*

An extensive net of ground measurements of wind and temperature from the Catalan Meteorological Service is available at the area of domain 4. Comparisons with these data are done by calculating the root-mean square error (RMSE), the BIAS and for the vector wind, the root-mean square vector error (RMSVE). Temperature at 2 m and wind at 10 m are evaluated.

Figure 10 shows the evolution of the RMSE and the BIAS for temperature at 2 m. Both statistics are calculated in basis to the observations. The errors in both simulations are nearly equal. The CORINE simulation is slightly warmer during night-time, as can be appreciated with the bias evolution, and slightly colder during daytime. The model is not able to reproduce the daily variations of the temperature, with an overestimation at night and underestimation during daytime.

The evolution of the RMSVE (figure 11) is similar with small differences. CORINE simulation gives little better results in RMSVE, but the RMSE of the magnitude of the velocity is slightly higher than in USGS results. The surface winds appear to be lower in CORINE simulation than in USGS one, and in both cases are lower than the observations during daytime, and higher at night. The evolution of RMSE and RMSVE for the wind shows a little improvement in wind direction with the CORINE land-use map.

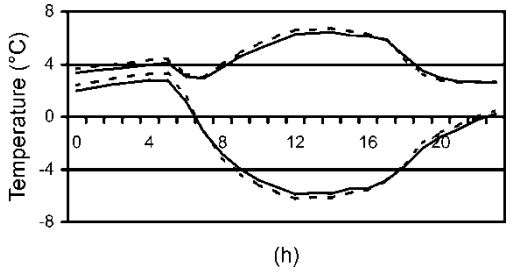

Figure 10. Daily evolution of the RMSE (upper curves) and the BIAS (bottom curves) for the temperature (°C) at 2 m (dashed line CORINE, solid line USGS).

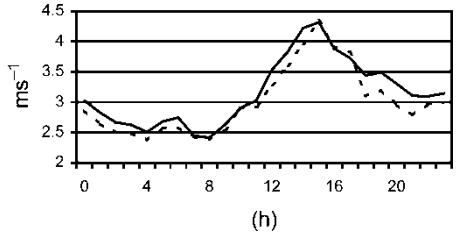

Figure 11. Daily evolution of the RMSVE for the winds (ms^{-1}) at 10 m (dashed line CORINE, solid line USGS).

7. Summary

An updating of the local physical parameters used in MM5 was intended, in order to get a better performance of the model and to have better regional simulations. Remotely sensed data of the year 2000 was used, as well as a recent land-use map. Results show that differences in surface parameters basically rely on thermal inertia. Besides, land-use map comparison had shown important differences between classifications that also affect the final composition of surface parameters that get into the model.

New values of the physical soil parameters have been introduced to MM5 with a new land-use map. These modifications have been sufficiently significant to produce variations in the performance of the model. The cloud development differs basically in the location and dimensions of the clouds, that drives to a different superficial radiative budget affecting the evolution of air temperature at low levels. The different results in cumulus simulation produced important differences in the surface wind field and the updrafts. The changes introduced are sufficiently significant to obtain slight variations in the pattern of accumulated precipitation for the simulated period.

Comparisons with ground measurements of wind and temperature have been done in the test regions. Similar errors are obtained with the two land-use maps and physical parameters, without a clear improvement in the performance of the meteorological model.

This work contributes evidence to the high influence of surface scheme in applications of mesoscale models at high horizontal resolution. In the context of a dialogue between remote sensing scientists and numerical climate modellers, it is expected that more research should be done to investigate the sensibility of mesoscale models to improvements in the surface properties characterization.

Acknowledgments

The authors wish to thank the Environmental European Agency for providing the EEA NATLAN-2000 land-use information package; the CREPAD-INTA (Instituto Nacional de Tècnica Aerospacial, Spain) for the NOAA-14 AVHRR data; the AUC-DLR Center (German Aerospace Center) for the NOAA-14 TOVS data; the VITO (Flemish Inst. Technological Research, Belgium) for providing the SPOT VGT S_{10} NDVI images; the Spanish Meteorological Institute (INM) for providing data from the ECMWF; and the Catalan Meteorological Service (SMC) for providing surface station data for validation. Simulations were run on an HP Exemplar V2500 belonging to CESCA (*Centre de Supercomputació de Catalunya*). This work was developed under projects IMMPACTE and CICYT REN2000-1754-C02-01/CLI.

References

ANDERSON, J. R., HARDY, E. E., ROACH, J. T., and WITMER, R. E., 1976, A land use and land cover classification system for use with remote sensor data: U.S. Geological Survey Professional Paper 964.

CHEN, F., and DUDHIA, J., 2001, Coupling an advanced land surface-hydrology model with the Penn State-NCAR MM5 modelling system. Part I: Model implementation and sensitivity. *Monthly Weather Review*, **129**, 569–585.

DERRIEN, M., FARKI, B., HARANG, L., LEGLÉAU, H., NOYALET, A., POCHIC, D., and

SAIROUNI, A., 1993, Automatic cloud detection applied to NOAA-11/AVHRR imagery. *Remote Sensing of Environment*, **46**, 246–267.

DUDHIA, J., 1993, A non-hydrostatic version of the Penn State-NCAR mesoscale model: validation tests and simulation of an Atlantic cyclone and cold front. *Monthly Weather Review*, **121**, 1493–1513.

EUROPEAN ENVIRONMENT AGENCY, 2000, CORINE Land Cover (1 : 100 000), NATure/LANd Cover information package. http://natlan.eea.eu.int

GOWER, J. C., 1971, A general coefficient of similarity and its properties. *Biometrics*, **27**, 857–871.

HOLBEN, B. N., ECK, T. F., SLUTSKER, I., TANRE, D., BUIS, J. P., SETZER, A., VERMOTE, E., REAGAN, J. A., KAUFMAN, Y., NAKAJIMA, T., LAVENU, F., JANKOWIAK, I., and SMIRNOV, A., 1998, AERONET – a federated instrument network and data archive for aerosol characterization. *Remote Sensing of Environment*, **66**, 1–16.

MESOSCALE AND MICROSCALE METEOROLOGY DIVISION, NATIONAL CENTER FOR ATMOSPHERIC RESEARCH, 2001, PSU/NCAR Mesoscale modeling system tutorial class notes and user's guide: MM5 Modeling system version 3, June 2001.

NOAA, 1998, Polar Orbiter Data User's Guide (November 1998 version) http://www2.ncdc.noaa.gov/docs/podug/index.htm

PRICE, J. C., 1977, Thermal inertia mapping: a new view of the earth. *Journal of Geophysical Research*, **82**, 2582–2590.

SAUNDERS, R. W., 1990, The determination of broad band surface albedo from AVHRR visible and near-infrared radiances. *International Journal of Remote Sensing*, **11**, 49–67.

SOBRINO, J. A., and EL KHARRAZ, M. H., 1999, Combining afternoon and morning NOAA satellites for thermal inertia estimation. 2. Methodology and application. *Journal of Geophysical Research*, **104**, 9455–9465.

SOBRINO, J. A., and RAISSOUNI, N., 2000, Toward remote sensing methods for land cover dynamic monitoring. Application to Morocco. *International Journal of Remote Sensing*, **20**, 353–366.

TEILLET, P. M., 1992, An algorithm for the radiometric and atmospheric correction of AVHRR data in the solar reflective channels. *Remote Sensing of Environment*, **41**, 185–195.

VALIENTE, J. A., NUNEZ, M., LOPEZ-BAEZA, E., and MORENO, J., 1995, Narrow-band to broad-band conversion for Meteosat-visible channel and broad-band albedo using both AVHRR-1 and -2 channels. *International Journal of Remote Sensing*, **16**, 1147–1166.

VALOR, E., and CASELLES, V., 1996, Mapping land surface emissivity from NDVI: application to European, African, and South American areas. *Remote Sensing of Environment*, **57**, 167–184.